Analyst

ROYAL SOCIETY OF CHEMISTRY

PAPER

Cite this: *Analyst*, 2021, **146**, 6506

Improvement of biomolecular analysis in thin films using *in situ* matrix enhanced secondary ion mass spectrometry†

Konstantin Moshkunov,[a] Benjamin Tomasetti,[a] Thomas Daphnis,[a] Vincent Delmez,[a] Kevin Vanvarenberg,[b] Véronique Préat,[b] Matthias Lorenz,[c,d] Jusal Quanico,[e] Geert Baggerman,[e,f] Filip Lemiere,[e,g] Christine Dupont[a] and Arnaud Delcorte *[a]

Received 26th April 2021,
Accepted 30th August 2021

DOI: 10.1039/d1an00727k

rsc.li/analyst

Sensitivity to molecular ions remains a limiting factor for high resolution imaging mass spectrometry of organic and biological materials. Here, we investigate a variant of matrix-enhanced secondary ion mass spectrometry in which the transfer of matrix molecules to the analyte sample is carried out *in situ* (*in situ* ME-SIMS). This approach is therefore compatible with both 2D and 3D imaging by SIMS. In this exploratory study, nanoscale matrix layers were sputter-transferred inside our time-of-flight (ToF)-SIMS to a series of thin films of biomolecules (proteins, sugars, lipids) adsorbed on silicon, and the resulting layers were analyzed and depth-profiled. For this purpose, matrix molecules were desorbed from a coated target (obtained by drop-casting or sublimation) using 10 keV Ar_{3000}^+ ion beam sputtering, followed by redeposition on a collector carrying the sample to be analyzed. After evaluating the quality of the transfer of six different matrices on bare Si collectors, α-cyano-4-hydroxycinnamic acid (CHCA) was selected for further experiments. The mass spectra and depth profiles obtained from the organic layer prior to and after the sputter-transfer of CHCA were compared, along with those obtained from regular ME-SIMS samples (dried droplets) and, finally, with MALDI data for the same matrix–analyte combinations. Signal amplification factors were calculated by dividing the integrated molecular intensities obtained with or without matrix transfer. While the amplification factors are between 0.5 and 2 for molecules already detected with high intensities in SIMS, such as cholesterol or human angiotensin, other compounds show very large integrated signal amplification, even above two orders of magnitude. This is the case for D-glucose and cardiolipin, for which the molecular ion intensity is low (or very low) under normal SIMS analysis conditions. For such low ionization probability compounds, the beneficial effect of the matrix is unquestionable. Test experiments on mouse brain tissue sections also indicate signal enhancement with the matrix, especially for high mass lipid ions.

1. Introduction

In recent years, secondary ion mass spectrometry, or SIMS, has evolved into a powerful molecular imaging technique, complementary to matrix-assisted laser desorption ionization (MALDI) MS[1] and ambient ionization approaches such as desorption electrospray ionization (DESI) MS.[2] In comparison with other methods, SIMS intrinsically possesses a better lateral resolution, because of the ability to finely focus ion beams and an unbeatable depth resolution, owing to the small size of the nanovolume excited by the projectiles, each of them forming a crater only a few nm deep in the sample surface.[3] With the advent of large gas cluster ion beams (GCIB),[4,5] 3D molecular imaging of tissues and cells has even been made possible.[6,7] On the other hand, it is well known that the ioniza-

[a]*Institute of Condensed Matter and Nanoscience, Université catholique de Louvain, 1 Place Louis Pasteur, 1348 Louvain-la-Neuve, Belgium.*
E-mail: arnaud.delcorte@uclouvain.be
[b]*Louvain Drug Research Institute, Université catholique de Louvain, Avenue Mounier 73, 1200 Woluwe-Saint-Lambert, Belgium*
[c]*National Physical Laboratory, Hampton Road, Teddington TW11 0LW, UK*
[d]*Present address: PerkinElmer Inc., 6-501 Rowntree Dairy Rd, Woodbridge, ON L4L 8H1, Canada*
[e]*Centre for Proteomics (CFP), University of Antwerp, Groenenborgerlaan 171, B2020 Antwerp, Belgium*
[f]*Flemish Institute for Technological Research (VITO), Boeretang 200, B-2400 Mol, Belgium*
[g]*Department of Chemistry, University of Antwerp, Groenenborgerlaan 171, 2020 Antwerp, Belgium*
†Electronic supplementary information (ESI) available. See DOI: 10.1039/d1an00727k

tion probabilities in SIMS vary strongly as a function of the considered element or molecule, but also depend on their chemical environment, so that the ion yields may vary widely for a given species placed in different samples.[8,9] This is often an issue for sensitivity and quantification, valid for biological samples as well irrespective of the chosen ion beam.[10,11] In general, sensitivity appears to be deceptively low for molecular ions of interest when imaging complex biological specimens partly because, with the improvement of the beam focus, useful signals have to be extracted from ever smaller volumes.[12]

One interesting strategy to overcome these effects, also valid for other mass spectrometries of solid samples, is to decouple desorption and ionization processes. For example, in electrospray-assisted laser desorption ionization (ELDI)[13] and laser-assisted electrospray ionization (LAESI),[14] lasers with different wavelengths ablate tissues in a section under atmospheric conditions, the molecular plume crosses a perpendicular electrospray jet and the resulting ionized species are entrained with the jet into the sampling skimmer of the mass analyzer. Other approaches rely on chemical ionization, photoionization (laser-SNMS[15] is a variant of SIMS), a flow of metastable helium atoms, or a laser plasma to ionize the molecules once they are in the gas phase.[16,17] While decoupling ionization from desorption circumvents the effect of the chemical environment in the solid sample, one still has to deal with low sensitivity to some classes of molecules.

Alternatively, a clever modification of the sample surface with carefully chosen ionizing agents may also constitute an interesting way to increase ionization in SIMS, and thereby address the sensitivity problem. *In situ* or *ex situ* surface modification approaches, including Cs implantation,[18] metal–organic salts,[19] glycerol,[20] ice[21] or metal condensation (metal-assisted SIMS),[22,23] water vapor dosing,[24] trifluoroacetic acid surface modification,[25] or organic (MALDI) matrix deposition (matrix enhanced-SIMS),[26] proved their potential for ionization enhancement, sometimes by orders of magnitude. ME-SIMS,[26–29] where acidic molecules generally act as proton donors for analyte ionization, proved unrivaled for the desorption-ionization of relatively large biomolecules using keV atomic projectiles. For instance, bovine ubiquitin (MW = 8565 Da), oligonucleotides (MW = 8157 Da) and cytochrome C (MW = 12 360 Da) were successfully desorbed and ionized by 2,5-dihydroxybenzoic acid (DHB) upon Cs^+ bombardment,[28] angiotensin and porcine insulin by α-cyano-4-hydroxycinnamic acid (CHCA) upon Xe^+ and SF_5^+ bombardment,[26] or gramicidin S (MW = 1141 Da) by sinapinic acid upon C_{60}^+ bombardment.[30] ME-SIMS functions very similar to MALDI,[31] using the same types of matrices, except for the laser being replaced with the ion beam. The disadvantage of such an approach is the formation of a charging matrix surface during ion bombardment and the loss of resolution when matrix crystals are over one micron in size.[29,32] Crystal heterogeneity was also recognized to affect the desorption–ionization efficiency.[33] Matrix sublimation alleviates some of the issues encountered with solution-based deposition,[29] and gives good results for 2D imaging of tissues.[34] However, it may lead to overheating of the biological sample and remains incompatible with 3D molecular imaging by SIMS. In order to conduct 3D molecular imaging experiments, *ex situ* surface treatments aimed at improving ionization are excluded, since they only affect the topmost surface layers and will be removed after a few cycles of surface erosion. One approach to enhance the molecular ion yields *in situ* involves the use of large clusters with specific chemistries as projectiles, such as water[35,36] Ar–CH_4 [37] or Ar–HCl clusters.[38] There is a link with ME-SIMS considering the hypothesis that these large cluster projectiles provide secondary ion enhancement *via* a transient matrix effect that lasts only the time of the interaction (ps). The process was coined "dynamic reactive ionization".[38]

Alternatively, the group of Prof. Ian Gilmore at the UK's National Physical Laboratory (NPL) reported a new strategy to form a matrix layer on an organic sample for ME-SIMS experiments.[39,40] They used the GCIB to transfer matrix molecules from a reservoir, called the target, to the analyte, deposited as a thin film on a collector plate. Prior to that study, the same group had demonstrated that antioxidant molecular ions (Irganox 1010) sputtered with 10 keV Ar_{2000}^+ clusters could be transferred essentially intact on a collector.[39] Indeed, the SIMS spectra measured on the target and the collector were extremely similar. We recently showed that biomolecules such as angiotensin, insulin and even lysozyme could also be transferred intact and even retain their bioactivity.[41,42] In this article, we add *in situ* a nanoscale matrix layer to thin films of biomolecules adsorbed on silicon and ultimately tissue sections, following the NPL transfer protocol. The original target-collector assembly was kindly provided by them and later on redesigned by us. The matrix is transferred from a coated target by GCIB sputtering, followed by redeposition on a collector carrying the sample to be analyzed. We compare the spectra and profiles obtained from the organic layer prior to and after the sputter-transfer, along with those obtained from classical ME-SIMS samples and, finally, with MALDI data for the same analyte–matrix combinations. In doing so, our main goal is to verify the feasibility and the performance of *in situ* ME-SIMS in comparison with regular SIMS (with no matrix), for the analysis of a series of model biomolecule samples and a real brain tissue section. Indeed, this *in situ* approach is fully compatible with 2D and also 3D molecular imaging. In addition, the transfer of a thin matrix layer by sputtering should also avoid overheating of the sample related to matrix sublimation, detrimental for tissue analysis.

2. Experimental methods

2.1. Sample preparation

The sample preparation and analytical protocols are summarized in Table 1. The substrates in most experiments were 0.3 mm thick [1, 1, 1] square-cut Si wafers (Neyco S.A., Vanves, France), except those for MALDI analysis and rodent brain tissue analysis. The Si substrates were cleaned with ethanol prior to use. All organic molecules were purchased from Merck

Table 1 Sample preparation and analysis protocols for the investigated methods

Method	Sample preparation	Analysis modes
ME-SIMS (Fig. 3–9)	Matrix : analyte solutions with a molar ratio of 500 : 1 were spin-coated	"Static" SIMS (30 keV Bi_5^+)
SIMS (Fig. 2 and 3–9)	• (Fig. 2) pure matrix drop-cast and sputter-transferred • (Fig. 3–9) analyte solutions spin-coated (no matrix)	• "Static" SIMS (30 keV Bi_5^+) • "Static" SIMS and depth profile (10 keV Ar_{3000}^+ for sputtering)
In situ ME-SIMS (Fig. 3–9 and 10)	• (Fig. 3–9) analyte solution spin-coated and matrix transferred *in situ* (10 keV Ar_{3000}^+ for sputtering) • (Fig. 10) tissue section embedded in CMC and matrix transferred *in situ* (10 keV Ar_{3000}^+ for sputtering)	• "Static" SIMS and depth profile (10 keV Ar_{3000}^+ for sputtering) • "Static" SIMS and depth profile (10 keV Ar_{3000}^+ for sputtering); 2D "mosaic" imaging
MALDI MS (Fig. 3–9)	1 μl of analyte solution spotted on a plate and 1 μl of matrix combined	Spectral acquisition and MS/MS measurements

(product numbers are given for each compound). Matrices were 2,5-DHB (85707), CHCA (70990), 1,5-DAN (56451), sinapinic acid (SA, 85429), THAP (91928), and 9-AA (92817). Analytes were maltoheptaose (M7753), angiotensin II human (A9525), L-α-phosphatidylcholine type XI-E (P2772), 3-*sn*-phosphatidylethanolamine from bovine brain (P7693), 14 : 1 cardiolipin sodium salt (710337C), cholesterol (C8667), D-serine (S4250), D-glucose (G8270), and D-glutamic acid (G1251).

Analyte solutions were 5 mg ml^{-1} in chloroform (lipids), acetonitrile : water 65 : 35 (maltoheptaose), and water (angiotensin, D-serine, D-glutamic acid, D-glucose). These solutions were spin-coated on Si substrates at 3000 rpm speed and 100 μl volume of solution to form reference analyte films. 2,5-DHB, THAP, SA, and 1,5-DAN were prepared as solution in water : acetonitrile (ACN) 1 : 1 and 9-AA as solution in methanol : water 9 : 1; also 2,5-DHB and CHCA were diluted in chloroform : methanol 2 : 1 solution for the experiments with lipids. For ME-SIMS measurements the matrix : analyte ratio was 500 : 1.

For the preparation of the mouse brain tissue sections, a cryopreserving protocol was applied in order to prevent the formation of ice crystals which would break cellular membranes and produce holes within the cells.[43] After collection, the mouse brain was immersed in a 4% paraformaldehyde (PFA) solution for 6–18 h at room temperature. Afterward, the PFA was replaced with a 10% sucrose solution at 4 °C until the sample sank in the vial. The same operation was repeated with a 30% sucrose solution. The sample was then placed in a plastic mold filled with carboxymethyl cellulose (CMC) that was immersed in isopentane chilled by liquid nitrogen. CMC is recognized as one of the best embedding media for SIMS analyses, shown to freeze a maximum amount of the different lipids (see ref. 44 and references therein). Once the CMC became white and homogeneous, the embedded sample was removed and either conserved in aluminum foil at −80 °C or directly cut using a cryomicrotome and the slices were deposited on glass slides. The brain tissue sections had a thickness of about 10 μm and were stored at −20 °C. In some cases, the sections were exposed for 30 minutes to trifluoroacetic vapor which is known to enhance/reveal the signal of high mass lipids.[25]

The matrix was deposited on the model biomolecular thin films in three ways – by drying a droplet of matrix–analyte mixture, by sputter-transfer *in situ* and by sublimation. For the experiments involving mouse brain tissue sections, only the last two approaches were tested in order to avoid molecular diffusion and thereby preserve their localization. Matrix sublimation was performed in a home-made vacuum apparatus where the sample was held on a copper head cooled by an ice-water slurry and the matrix crucible was heated from the atmospheric side using electric heaters, which were PID-controlled by a device with a temperature sensor in the crucible. The time–temperature values for controlled sublimation were initially taken from ref. 34 and then adjusted so that reproducible matrix layers could be grown in a 50 nm to 10 μm range. Targets for sputter-transfer (*in situ* ME-SIMS) had 5 μm thick matrix layers, which took approximately 3 hours to erode with a 5–10 nA sputter beam scanned over a 1 × 3 mm^2 spot. For *in situ* ME-SIMS, the matrix layer was fully transferred only once, before depth profiling. Note that the duration of the matrix transfer could be very significantly reduced for future applied studies: (i) larger beam currents and an optimized compromise regarding the most appropriate cluster size can be attained; (ii) the geometry should be optimized (75° incidence on the target is not optimal for the sputtering yield[39]); and (iii) the ~60 nm of matrix transferred for this study might not be needed since static SIMS reaches maximum intensities with less than 10 nm of material (crater depth of a Bi_{3-5}^+ impact is about 5 nm).

Sublimation was found to be a very good way to produce homogeneous layers with minimal surface roughness (tens of nanometers) on the targets used for sputter-transfer (*in situ* ME-SIMS). Indeed, the crystals formed by drying a droplet of matrix solution were irregular and often spiky with characteristic sizes of tens of microns.[45] The latter did not perform well as targets for *in situ* ME-SIMS due to very intense charging and little of the material being transferred to the collector compared to the sublimated matrix targets. However, dried droplets had the desired matrix to analyte ratios and were used to measure reference spectra by ME-SIMS and MALDI. As a possible alternative to sublimation, matrix applied with specific sprayer devices also produces submicron crystals, adapted for high-resolution 2D imaging, which could be of interest to produce uniform matrix targets for *in situ* ME-SIMS.[46]

2.2. Time-of-flight secondary ion mass spectrometry and ion beam transfer setup

The main instrument is a TOF.SIMS 5 machine (IONTOF GmbH, Münster, Germany), equipped with both Bi(Mn) NanoProbe-LMIG (liquid metal ion gun) and Ar-GCIB (gas cluster ion beam) primary ion sources providing beams oriented at 45° to the surface normal. Depth-profiling experiments were conducted in the dual-beam mode. A 10 keV Ar_{3000}^+ beam was used for the sputtering of the target (matrix transfer) and for the sputtering of the samples in the depth profiling experiments. A 30 keV Bi_5^+ pulsed beam was used for spectral analysis with a raster area of 500 × 500 μm^2 and an ion fluence per analysis point always well below 10^{12} ions per cm^2 (static conditions). Each presented SIMS spectrum is representative of three independent measurements and depth-profile experiments were reproduced two to five times depending on the samples. The geometry of the ion beam columns and the extraction system is fixed, therefore we had to adapt to it for the sputter-transfer experiments, as shown in Fig. 1. The collector with the analyte sample had to be horizontal for the extraction system to be able to collect secondary ions from it, while the sputtered target was tilted to have the sputtering beam at a 15 degree incidence angle (to the surface), so that the ejection in a mirror direction is towards the closest part of the collector/sample. The same geometry was used by Lorenz *et al.*[40]

For the collector analysis, the matrix-covered surfaces were often non-conductive and led to charge build-up in the depth-profiling mode. Nevertheless, we decided to avoid electron flooding compensation as it is not localized or focused on just the analytical area but rather covers the whole surface of the target and sample, and because electrons even at 10 eV may cause non-negligible degradation of complex organic molecules, as was noticed in our preliminary experiments. Some of our samples proved to be charging and some were conductive, so a uniform approach had to be developed for both types to enable a direct comparison of spectra. To deal with the charging in the depth-profiling experiments, the sputtering beam average flux was reduced tenfold by shortening the exposure time to the sputtering beam during the analytical cycle. For a 200 μs total cycle duration, the sputtering beam was enabled at 20 μs and switched off at 60 μs so that the surface charge could recover for the remaining 140 μs. The Bi_5^+ analysis current was about 0.05 pA and the GCIB sputtering current was 0.4 nA.

For the analysis of brain tissue sections (Fig. 10), the depth profiles were obtained with a 10 keV Ar_{3000}^+ sputter current of 3 nA and a 30 keV Bi_5^+ analysis current of 0.1 pA. The total sputtering fluence was 4.87 × 10^{15} ions per cm^2. 20 eV electrons (floodgun) were used for charge compensation. Finally, the large area 2D images of brain samples (inset of Fig. 10c) were acquired using 30 keV Bi_5^+ primary ions with a current of 0.07 pA. The total area of 10 × 7 mm^2 was divided into small patches of 500 × 500 μm^2 where 4 frames were acquired for each one. The cycle time was set to 110 μs to allow high mass lipid detection.

2.3. Matrix-assisted laser desorption ionization

Mass measurements were performed using a RapiFlex tissuetyper (Bruker Daltonics, Bremen, Germany). This MALDI-TOF instrument is equipped with a Smartbeam™ 3D laser with a laser diameter of 5 μm and capable of firing at a maximum repetition rate of 10 kHz. Depending on the experiment, the instrument was set in the positive or negative or linear or reflector mode. The parameters for each mode, such as the voltages for ion acceleration, sampling rate, detector settings and pulse ion extraction delays, are shown in ESI Table 1.†

Depending on the sample, external calibration was performed using PepMix 6 (LaserBio Labs, Sophia-Antipolis, France), peptide mass calibration standard II, or protein mass calibration standard I (Bruker Daltonics). 1 μL of each sample was spotted on a stainless steel plate and 1 μL of the appropriate matrix (2,5-DHB for lipids, amino acids and sugars prepared at 10 mg mL^{-1} in 70% methanol/0.1% trifluoroacetic acid (TFA) in water, CHCA for peptides prepared at 7.5 mg mL^{-1} in 70% ACN/0.1% TFA in water, and SA for intact proteins prepared at 10 mg mL^{-1} in 70% ACN/0.1% TFA in water) was combined and dried under vacuum.

MS/MS measurements were performed on the Sciex 4800+ MALDI TOF/TOF instrument (AB Sciex, Nieuwerkerk aan den Ijssel, Netherlands) operating in the positive reflector mode. The relative resolution of the precursor mass window was set at 200 FWHM. The laser intensity was fixed at 6500, and a total of 3000 laser shots were acquired per spectrum. Metastable suppression was activated. The digitizer bin size was set at 0.5 ns. The voltage parameters are given in ESI

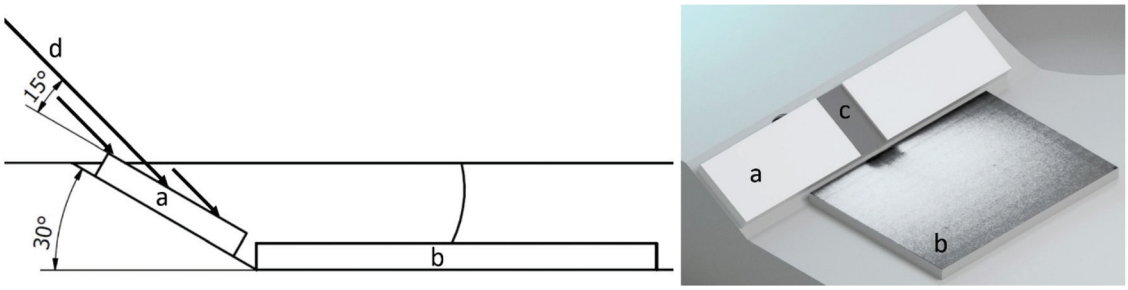

Fig. 1 Experimental geometry for sputter-transfer experiments: (a) target, (b) collector, (c) sputtered area, (d) sputtering beam.

Table 2.† The sample was prepared in the same manner using the same matrix as in the Rapiflex measurements.

3. Results and discussion

3.1. MALDI matrix transfer

In this section, the results are presented in the same order as the study progressed. After deciding on the *in situ* matrix transfer and stage design, we proceeded to test how well the different matrices were performing in the transfer process. For this purpose, targets were prepared with the following matrices on them (dried droplets): 2,5-DHB, CHCA, THAP, 9-AA, 1,5-DAN and SA. They also constituted our reference samples for the pure matrix. The targets were sputtered for several hours and the collectors were 1×1 cm^2 Si squares. Positive ion mass spectra were acquired from the reference matrix samples and from the material that was deposited on the collectors (Fig. 2). The mass spectra of the reference samples provide (a) the peak of the matrix molecule either in the protonated or ionized form ($[M + H]^+$ or M^+), (b) the main fragment often resulting from H_2O loss and (c) multimers of the matrix. The comparison reveals how well the transferred matrix retains the peak distribution. In general, it is difficult to compare the measured intensities since the reference and transferred matrices have very different crystal morphologies and overall thicknesses.

Starting with 2,5-DHB (Fig. 2a), the mass spectrum of the transferred matrix completely loses the peak of the original molecule, while preserving the main fragment ion with a very high intensity. This observation is probably due to the sublimation of 2,5-DHB in a vacuum as demonstrated in ref. 47, where a 80 nm thick matrix layer disappeared after half of a day of exposure to ultra-high vacuum. Our process cycle is several hours long and the estimated final layer thickness should be approximately half of the one mentioned in the article by Körsgen *et al.* Because they likely reach the collector as radicals, the transferred fragments of 2,5-DHB might,

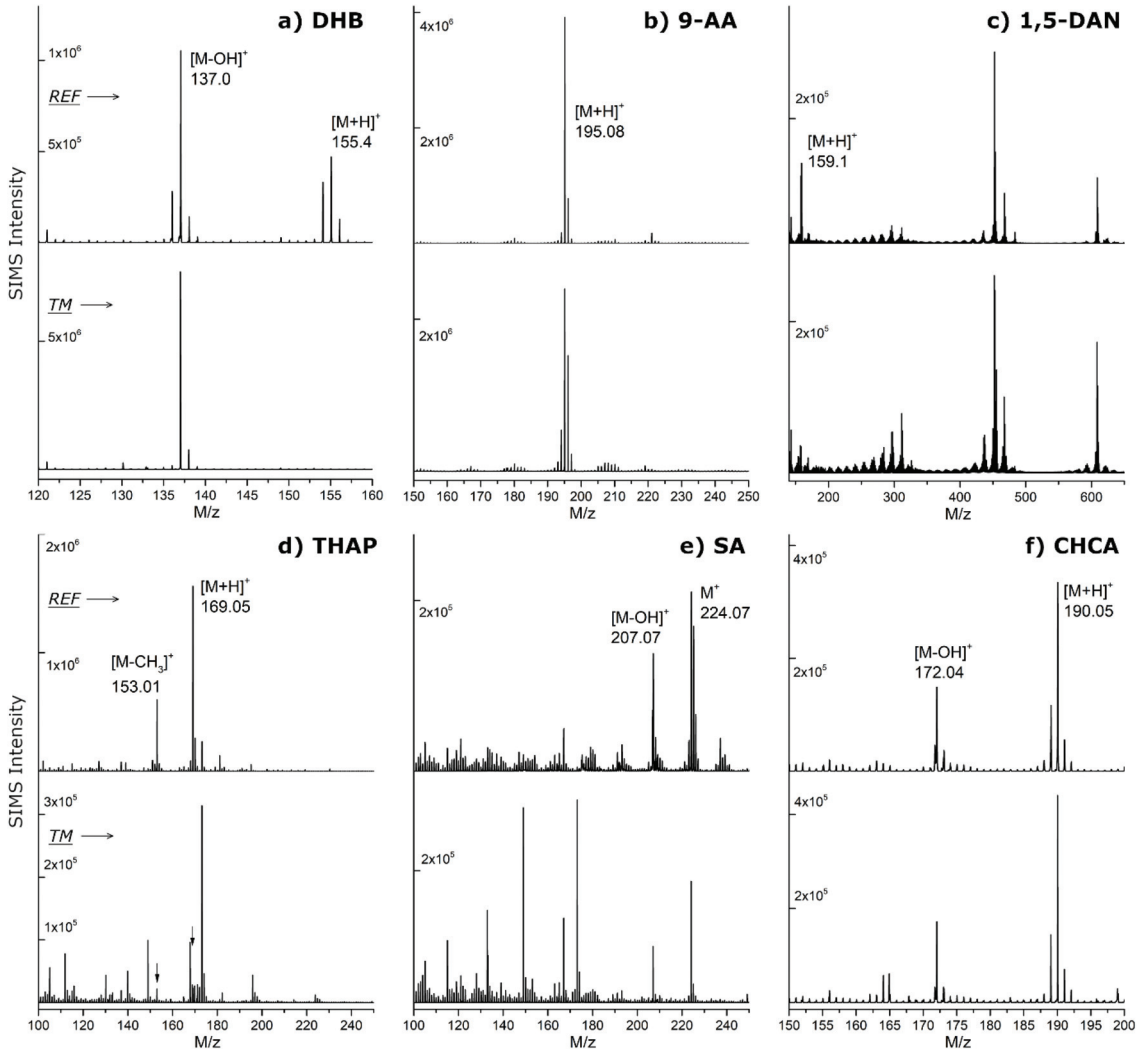

Fig. 2 Partial positive ion mass spectra for reference samples and sputter-transferred matrices: (a) 2,5-DHB, (b) 9-AA, (c) 1,5-DAN, (d) THAP, (e) SA and (f) CHCA. The upper spectra correspond to the reference samples (*REF*), while the lower ones to the transferred matrix (*TM*).

however, react to form a more stable bonding with the surface. 2,5-DHB matrix sublimation might not be a critical problem in MALDI because the deposited layers are usually much thicker (in the μm range). In contrast to 2,5-DHB, 9-AA shows no signs of degradation upon transfer, with the protonated monomer being the dominant peak (Fig. 2b). Transferred 1,5-DAN poorly preserves the main peak, but the dominant species in the spectrum are oligomers and they retain their pattern well, thus we consider the transfer to be successful (Fig. 2c). THAP exhibits a dramatic loss of intensity for both the protonated molecule and the main fragment ion, compared to the rise of lower mass background fragmentation (Fig. 2d). Sinapinic acid displays an intermediate behavior, with the main peaks being retained, albeit with some intensity reduction, and a significant increase of the fragments in the spectrum (Fig. 2e). Finally, the transfer of CHCA proved to be successful, with the transferred matrix spectrum very similar to the reference (Fig. 2f).

For the reference and the transferred target spectra shown in Fig. 2, all matrices were drop-cast, resulting in visible crystal sizes, which do not work very well with grazing incident beams. To quantify the importance of roughness, similar transfer experiments were carried out with sublimated targets (2,5-DHB, CHCA) which had >5 μm thickness of very homogeneous and flat matrix layer (~10 nm roughness) and the resulting mass spectra had the same peak distributions as those obtained using drop-cast samples. The noticeable difference was in the thickness of the layer deposited on the collector for a given GCIB dose. Indeed, targets with sublimated matrix resulted in a significant increase of the transferred layer thickness, from a few nanometers to approximately 50 nm.

The next stage of the study was to compare the structure and intensities of the mass spectra obtained for different coatings of biomolecules, each prepared in the form of ME-SIMS samples, reference spin-coated samples, reference spin-coated samples with an overlayer of *in situ* transferred matrix (sputter-coated) and MALDI samples (see Table 1). The initial choice of organic mixtures would require a preliminary study of the general effectiveness of each matrix to enhance the detection of each analyte and then building the mass spectra database to perform the aforementioned comparison. However, because of time and equipment access constraints, only a selection of combinations were studied. In addition, each matrix would require a calibration study for the matrix sublimation device to work reliably, therefore the spectral comparison part was limited to one matrix type. This decision is reasonable considering that any target of interest, an organic tissue slice for example, would be coated by one type of matrix at a time. 2,5-DHB and CHCA are the most likely candidates from the point of view of their widespread use for biomolecule ionization in MALDI. However, our preliminary study showed that 2,5-DHB matrix transferred with the GCIB did not result in the detection of intact molecules on the collector, probably because of its evaporation rate in UHV. Considering the analyte classes in our study, the quality of the sputter-transfer (Fig. 2) and the matrices predominantly used in the field, our choice for the remainder of this study was CHCA.

3.2. MALDI matrix transfer to organic layers

In this section, we successively present and discuss the effect of the *in situ* sputter-transfer of an overlayer of matrix on a series of analyte coatings of biological relevance. For each analyte, the spectral comparison is plotted in the following order (Fig. 3–9): (a) ME-SIMS, (b) SIMS of the reference sample (static), (c) SIMS of the sputter-coated reference sample, *i.e. in situ* ME-SIMS (mass spectrum corresponding to the total profile) and (d) MALDI MS. The bottom graph of the figure, (e) is a logarithmic depth profile for the reference sample and the *in situ* ME-SIMS sample. It also indicates the level of peak intensities for the reference sample in the static SIMS measurement. The profiles are color-coded with Si represented by a black line, the CHCA signal in blue and the analyte in red or multi-colored line (see annotations on the graphs), while dashed lines indicate static SIMS levels and reference sample profiles.

The sputter time was converted into depth using the volumetric sputtering yield of CHCA Y_v = 48 ± 5 nm^3 to convert primary ion fluence into equivalent thickness (thickness [nm] = fluence [ions per cm^2] × Y_v [nm^3] × 10^{-14}). This yield was obtained by comparing the thicknesses of pure sublimated

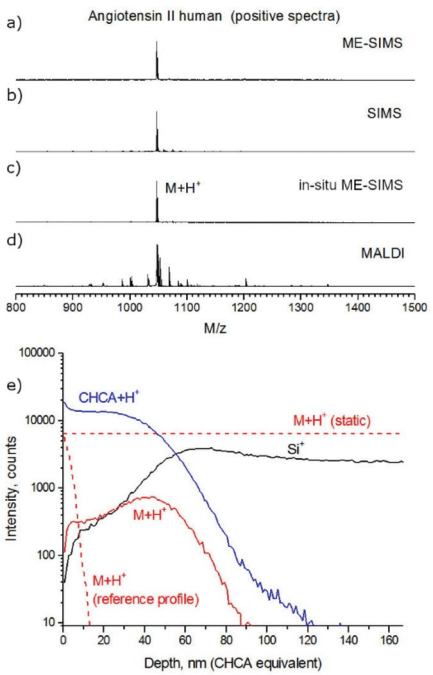

Fig. 3 Spectral comparison chart (a–d) and depth profile (e) for angiotensin II human. In (e), the profiles obtained on *in situ* ME-SIMS samples are color-coded with Si, CHCA and analyte signals being represented by solid black, blue and red lines, respectively. The dashed horizontal red line indicates the pseudo-molecular ion level attained for a static SIMS analysis and the dashed oblique red line for the depth profile, both for the reference sample.

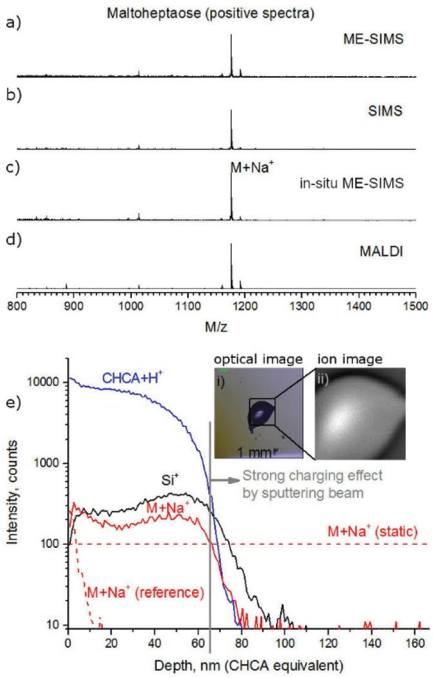

Fig. 4 Spectral comparison chart (a–d) and depth profile (e) for a maltoheptaose crystal. The explanation of (e) is the same as that in Fig. 3.

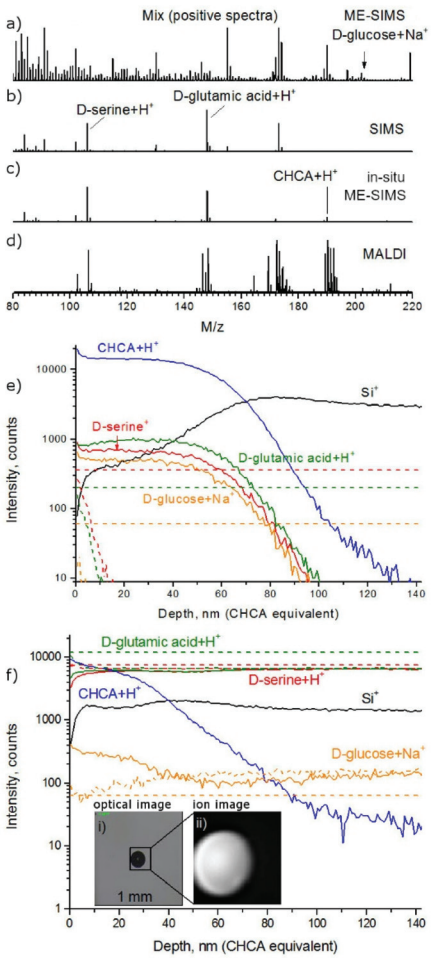

Fig. 5 Spectral comparison chart (a–d) and depth profiles for the mixture of D-serine, D-glucose and D-glutamic acid obtained for (e) flat area and (f) solid droplet. In (e) and (f), the profiles obtained on *in situ* ME-SIMS samples are color-coded with Si and CHCA being respectively represented by solid black and blue lines. The pseudo-molecular ions of D-serine, D-glucose and D-glutamic acid are in red, orange and green, respectively. The dashed horizontal lines with the same color coding indicate the pseudo-molecular ion levels attained for a static SIMS analysis and the dashed oblique lines for the depth profile, both on the reference sample.

matrix layers measured using a profilometer and the fluence of 10 keV Ar_{3000}^+ cluster ion beam required to erode the layer. The derived time-to-depth conversion coefficient was used on all profiles, even for pure analyte layers, even though the sputtering of organic layers by large cluster beams may vary significantly for Ar clusters with an energy of ~3 eV per atom.[48,49] The CHCA equivalent thickness scale should be valid in the matrix layer, where analytes are strongly diluted, but it should only be considered as a crude approximation in the analyte layer and is obviously meaningless for the Si substrate.

The first compound is angiotensin II human (Fig. 3). This peptide already provides a strong $[M + H]^+$ signal from the reference sample and no intensity gain is observed with the transferred matrix. The spin-coated layer is a few nanometers thick, the matrix layer is *ca.* 60 nm thick and the analyte signal is distributed along the depth with an expected loss of magnitude due to dilution. Two hypotheses can be made to explain the Si^+ residual signal coming from the matrix layer. The most obvious reason would be that there are pinholes in the organic film. Imaging SIMS experiments conducted by Körsgen *et al.* on 2,5-DHB layers deposited on silicon by sublimation demonstrate that the Si substrate signal can be detected even with a matrix layer thickness of 80 nm, indicating the presence of such pinholes.[47] In our case, there is a slight possibility that silicon could be transferred from the target edges, where the substrate might be exposed to the sputtering beam, to the collector with the matrix flux. Indeed, with the very oblique incidence of the Ar cluster beam on the target, the area scanned by the beam is difficult to adjust precisely. The sputter yield of Si (SiO_2) for Ar cluster ions with an energy of ~3 eV per atom is low but it is not zero and therefore this hypothesis cannot be directly discarded.[48,50]

The next compound is maltoheptaose (Fig. 4). The spin-coating leaves several solid droplets on the surface, which contain maltoheptaose, while no traces of it were found on the surrounding flat surface. The presented data is for the droplet area only as illustrated in the profile inset showing the optical and ion images of the sputtered and analysis areas, respectively. Different types of detection processes again produce very similar spectra with the sodiated main peak, but the profile behaves differently. The reference profile shows an abrupt drop in intensity, not due to the exhaustion of the molecular layer as was the case for the angiotensin thin layer (Fig. 3), but due to the strong charging effect of the solid maltoheptaose.

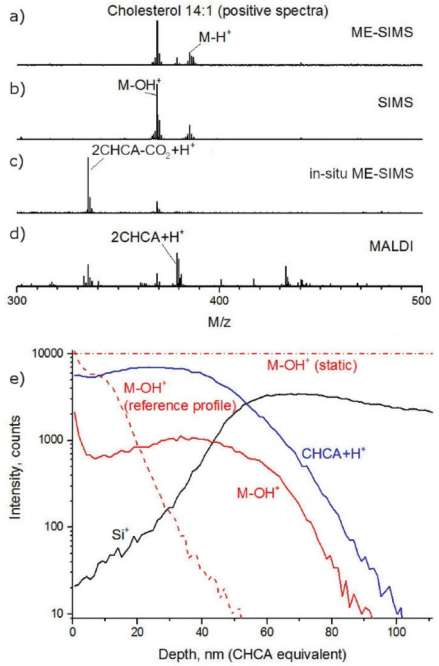

Fig. 6 Spectral comparison chart (a–d) and depth profile (e) for cholesterol. The explanation of (e) is the same as that given in Fig. 3.

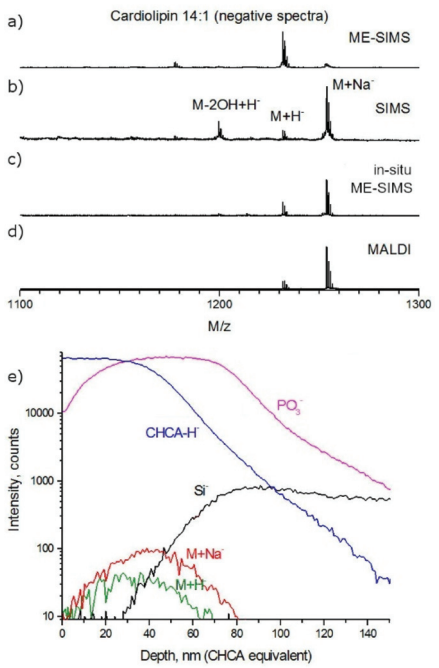

Fig. 7 Spectral comparison chart (a–d) and depth profile (e) for the cardiolipin 14 : 1 sodium salt. In (e), the profiles obtained on *in situ* ME-SIMS samples are color-coded with Si, CHCA, M + Na, M + H and PO_3 signals being represented by solid black, blue, red, green and pink lines, respectively.

Indeed, as shown in Fig. 3, the decay of the molecular signals is accompanied by an increase of the Si^+ signal, indicating the total sputtering of the organic layer, while, as shown in Fig. 4,

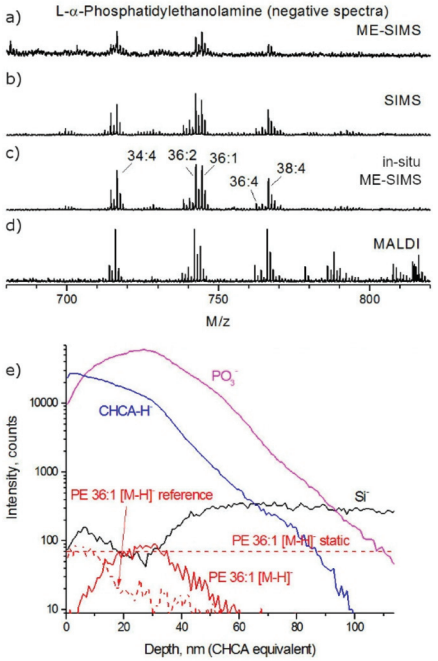

Fig. 8 Spectral comparison chart (a–d) and depth profile (e) for the L-α-phosphatidyl-ethanolamine mixture. In (e), the profiles obtained on *in situ* ME-SIMS samples are color-coded with Si, CHCA, PE 36 : 1 and PO_3 signals being represented by solid black, blue, red and pink lines, respectively. The dashed red lines have the same meaning as in Fig. 3.

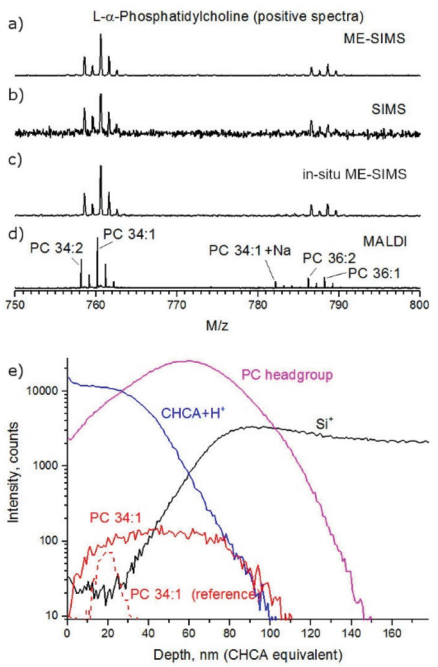

Fig. 9 Spectral comparison chart (a–d) and depth profile (e) for the L-α-phosphatidylcholine mixture. In (e), the profiles obtained on *in situ* ME-SIMS samples are color-coded with Si, CHCA, PC 34 : 1 and PC headgroup signals being represented by solid black, blue, red and pink lines, respectively. The dashed red line indicates the pseudo-molecular ion level attained for the depth profile on the reference sample.

all signals including those of Si^+ level off because of charging, even though the maltoheptaose droplet material is far from exhausted. The charging effect is also visible in the changing shape of the peaks in the mass spectra. The sample with the transferred CHCA layer provides a good level of stable signal in the matrix, with an analyte signal intensity that is higher than the static signal, clearly indicating the signal enhancement by CHCA. It is remarkable that charging seems to start only when the beam reaches the solid maltoheptaose drops in the matrix-covered sample, while the ion signals are maintained across the matrix layer. This suggests that the ~60 nm CHCA matrix constitutes a medium apt to mitigate the charging effect and enable analysis without electron flooding with our rather mild conditions of molecular depth profiling (see the Experimental section).

In the next experiment we used a mixture of three light analytes: D-serine, D-glucose and D-glutamic acid, which are often recognized as metabolites. Fig. 5 shows the spectra chart and the results obtained for the flat surface and for a solid droplet were similar to those found on the maltoheptaose sample, but smaller in size. This time, the mass spectra chart indicates a strong contrast between MALDI and ME-SIMS. The latter contains a number of peaks in the 100–200 Da mass region and the protonated peaks of D-serine and D-glutamic acid are weak in comparison with SIMS or MALDI. The background signal may be attributed to the extensive fragmentation induced by the Bi_5^+ 30 keV analysis beam, and is always present in SIMS analysis. Static SIMS and MALDI detect all these compounds well, as well as *in situ* ME-SIMS. D-Glucose is detected in a sodiated form, as expected. The spin-coated layers are a few nanometers thick and matrix coating drastically improves the signal intensity (Fig. 5e). Additionally, we performed the analysis of solid droplets found on the surface, see Fig. 5f. These droplets do not exhibit charging like those of maltoheptaose and seem to be mainly composed of D-serine and D-glutamic acid with little trace of D-glucose. The former molecules produce very intense peaks reaching the same level as CHCA. The sensitivity in this case is slightly reduced by the matrix overlayer for the former two molecules. The rather intense Si signal comes from the solid surface around the spot.

Thus here is an example of how matrix can facilitate species detection at a low concentration (thin layer, Fig. 5e) and hinder it for a saturated medium (droplet, Fig. 5f). We speculate that the different matrix : analyte ratios in these two configurations might be the cause of the observed differences. When the reservoir of the analyte is really large such as in droplets (virtually infinite, Fig. 5f), the added molecules of matrix may not increase ionization substantially because the matrix : analyte ratio might remain too low in the overlayer. On the other hand, thin analyte layers (Fig. 5e) can only provide a limited number of molecules to the matrix overlayer and therefore the matrix : analyte ratio should reach larger values, resulting in embedding of the analyte in the matrix that is optimal for ionization enhancement.

The next items on the list are lipids, namely cholesterol (Fig. 6), cardiolipin (14 : 1) (Fig. 7), a mixture of L-α-phosphatidylethanolamines (Fig. 8) and a mixture of L-α-phosphatidylcholines (Fig. 9). In SIMS, cholesterol is easy to detect *via* its $[M - H]^+$ peak (*m*/*z* 385.3) and its main fragment $[M - OH]^+$ (*m*/*z* 369.4).[51] The MALDI spectrum, however, misses the $[M - H]^+$ peak, while the ME-SIMS spectrum detects both. The spin-coated layer of cholesterol was found to be 10–15 nm thick, providing a good reference profile. The mixing of this layer with the deposited matrix causes a severe loss of signal, even if the signal is integrated over the entire profile. An intriguing additional feature is visible in the considered mass range of the spectrum. The CHCA matrix in any form (transferred, mixed or sublimated) produces a dimer signal of $[CHCA_2 + H]^+$ at *m*/*z* 379.1. However, in *in situ* ME-SIMS and MALDI, an additional peak is present at *m*/*z* 335.15, which is identified as $[CHCA_2 - CO_2 + H]^+$, possibly the reaction of two CHCA molecules accompanied by the elimination of a carboxylic acid residue. This peak is absent from the ME-SIMS measurement. In the *in situ* ME-SIMS case it could be due to the fragmentation of the original matrix transferred on the collector upon GCIB sputtering, followed by the reaction of the fragments with intact molecules on the collector surface (reactive landing). In MALDI, one must assume another route, *e.g.* the reaction of excited matrix molecules in the plume followed by CO_2 elimination, or the fragmentation of a CHCA molecule (direct photo-dissociation or post source decay) followed by the reaction of the fragment with another matrix molecule in the plume. Both of these mechanisms involve reactions in the dense ablation plume. The cluster impact, as demonstrated by molecular dynamics simulations, is faster (a few picoseconds) and the energized volume is orders of magnitude smaller in size (~10^3 nm^3).[3,41] The sputtered molecules are mostly generated at the rim of the impact crater and they experience much less collisions with each other than molecules in the denser and much larger MALDI plume. Therefore such complexes are unlikely to be formed in ME-SIMS but are present in the MALDI analysis. Collisions in the plume are also central to the proton transfers and charge exchange processes that make matrices so effective,[52] which might explain why ME-SIMS and MALDI results are sometimes different.

Cardiolipins (CL) represent an important class of mitochondria-specific anionic glycerophospholipids, which exhibit multiple structural and functional roles related to mitochondrial signaling, bioenergetics, and cellular death pathways. In this study, CL was supplied as a sodium salt and produces several molecular peaks in both positive and negative ion polarities. Fig. 7a–d show the negative ion mass spectra, as they are less fragmented and offer better sensitivity than the positive ones. The purchased cardiolipin salt contains two sodium atoms and therefore it naturally produces an intense quasi-molecular ion peak in the negative ion mass spectrum corresponding to the loss of a sodium cation. Here, the non-sodiated cardiolipin is denoted as M and, following this convention, then the common peaks are $[M + Na]^-$ and $[M + H]^-$ (exchange of Na by H in the cardiolipin salt). While the *in situ* ME-SIMS and MALDI spectra are almost identical, ME-SIMS displays an

inversion of these peak intensities. The SIMS signal comes with the peak identified as $[M - 2(OH) + H]^-$ but it is worth noticing that the static SIMS spectrum showed so little signal that it took a full hour of accumulation in order to identify these peaks. In consequence, the profile shown in Fig. 7e lacks the reference profile and the static value as they are at the noise level (<10 counts). *In situ* ME-SIMS reveals the presence of CL in the matrix, with an integrated intensity that is orders of magnitude larger than that of the reference SIMS spectrum. In the profile of PO_3^-, an intense fragment ion coming from the CL molecule, is also reported. With a much better signal-to-noise ratio than the pseudomolecular ion, it confirms the distribution of CL molecules in the matrix layer.

The negative mass spectra of the phosphatidylethanolamine (PE) mixture (Fig. 8) contain a large number of peaks. Both negative and positive (not shown) ion mass spectra are similar for the different methods involved. However, the ME-SIMS spectrum (Fig. 8a) shows a rather low signal-to-noise ratio in comparison with the others. Perhaps the drop-casting led to the distribution of the analyte inside the big crystals rather than at their exposed surface, only accessible to static SIMS. The detailed data processing of the MALDI spectra allowed us to identify only some of them as PEs (marked in the negative *in situ* ME-SIMS spectrum shown in Fig. 8c). These were confirmed by MS-MS analysis and then used to identify peaks in the SIMS-related mass spectra. The species in question shows both protonated and sodiated molecular peaks in the positive polarity and only deprotonated molecular ion peaks in the negative polarity. Combining all the information, some chain lengths and saturation combinations could be identified and others ruled out. PE 36 : 1 has a high intensity and since the PE peak distribution does not change its shape upon depth profiling, it is representative of the signal evolution over the whole profile shown in Fig. 8e. Interestingly, the maximum signal intensities and the integrals differ little between the reference and the *in situ* ME-SIMS profiles. This is true in both the negative and the positive polarities, therefore, only one of them is shown here.

Finally, the phosphatidylcholine (PC) mixed samples have quite similar mass spectra as the PE mixed samples (Fig. 9), except for a very intense fragment peak corresponding to the PC headgroup (*m*/*z* 184.1).[53] The static SIMS spectrum contains very little PC signal and a long acquisition period was required to identify the peaks. The depth profile of the reference coating reveals a buried PC layer of approximately 30 nm thickness. The *in situ* ME-SIMS depth profile has a slightly larger maximum intensity, but a significantly better integrated intensity which, considering a several-fold dilution of the sample by the matrix layer, indicates a strong enhancement of sensitivity (Fig. 9e).

Some of the above results are summarized in Table 2, which shows the values (in counts) of the displayed mass peak integrals calculated from the SIMS depth profiles of the reference samples (pure biomolecule film) and from the profiles of the samples covered by matrix transfer *in situ* (*in situ* ME-SIMS). Also the maximum spectral intensity (counts per s) is given for both experiments. The ratio of matrix-enhanced and reference integrals is the detection amplification induced by the matrix.

The results show that the amplification factors are between 0 and 1 for lipids such as cholesterol and the PE mixture, indicating that the application of the CHCA matrix does not offer any improvement in the detection for these compounds. It is not an issue in the case of cholesterol because this lipid is detected with very high intensity in the SIMS spectra, as was shown in a multitude of tissue imaging SIMS studies prior to this work.[53,54] A partial suppression of the cholesterol ions due to the presence of a matrix on the sample was also shown in the case of DHB.[54] However, the case of PE molecules is more annoying, since their intensities are naturally rather low in SIMS. The positive effect of the CHCA matrix is much clearer for PC lipids with an amplification of the integrated signal close to one order of magnitude. Some other compounds show very large integrated signal amplification, even above two orders of magnitude, such as D-glucose and cardiolipin deposited as thin layers, for which the intensity is very low under normal SIMS analysis conditions. For such compounds with a low probability ionization, the beneficial effect of the matrix is unquestionable. In these results, the signal enhancement is generally much larger when integrated over the entire matrix layer thickness, rather than static SIMS spectra, which

Table 2 Maximum spectral intensities and integrals calculated from the depth profile experiments for reference and matrix-covered samples. Values are rounded up to two significant digits. Data for metabolites are taken from the flat part of the sample surfaces

Compound	Ion	*m*/*z*	Max. spectral intensity (cps) *Reference*	Max. spectral intensity (cps) *In situ* ME-SIMS	Integral (counts) *Reference*	Integral (counts) *In situ* ME-SIMS	Amplification factor (ratio of the integrals)
L-α-PC	$(M + H)^+$	760	70	160	1100	9800	8.9
L-α-PE	$(M - H)^-$	744	90	90	2000	2000	1
Cardiolipin salt	$(M + Na)^-$	1254	5	100	5	4100	820
Cholesterol	$(M - OH)^+$	369	11 000	2100	83 000	46 000	0.55
D-Serine (thin layer)	$(M + H)^+$	106	360	870	1400	45 000	32
D-Glucose (thin layer)	$(M + Na)^+$	203	60	670	100	33 000	330
D-Glutamic acid (thin layer)	$(M + H)^+$	148	200	1100	700	64 000	91
Maltoheptaose	$(M + Na)^+$	1175	260	330	—	—	—
Angiotensin h. II	$(M + H)^+$	1046	6500	760	18 000	30 000	1.67

is made possible only because damageless depth-profiling can be performed owing to large Ar clusters.

Finally, an overlayer of the CHCA matrix was transferred *in situ* on a mouse brain tissue section (Fig. 10). Fig. 10a shows a depth profile experiment similar to those presented previously, going through the matrix (in blue, marked M) and then in the tissue itself (marked T), about halfway into the profile. The cholesterol signal obviously migrates into the matrix layer, as was also observed in Fig. 6 for a pure cholesterol layer and, to some extent, higher mass lipids do so too, as exemplified by the sodiated molecular ion of PC 32 : 0 at *m*/*z* 756.5. The difference of the cholesterol and higher mass PC profiles suggests that cholesterol diffuses more or faster to the surface, as previously investigated by several authors.[29,54,55]

Images were reconstructed from the two parts of the profile marked M and T, with the same number of analysis cycles (Fig. 10b). They show signal enhancement for cholesterol, PCs and also the phosphocholine headgroup. So the dilution of those species in the matrix provides larger molecular and fragment ion signals than their dilution in the tissue section. Fig. 10c shows a comparison of the high mass range of the positive SIMS spectra obtained on an untreated brain tissue section (RT) and on a similar section covered with CHCA (M) for a comparable primary ion dose, showing the remarkable enhancement in this mass range. The inset is a large area image of the brain section covered with *in situ* transferred CHCA (after TFA treatment), with the localization of the galactocerebroside 42 : 1 through its adduct with sodium on the

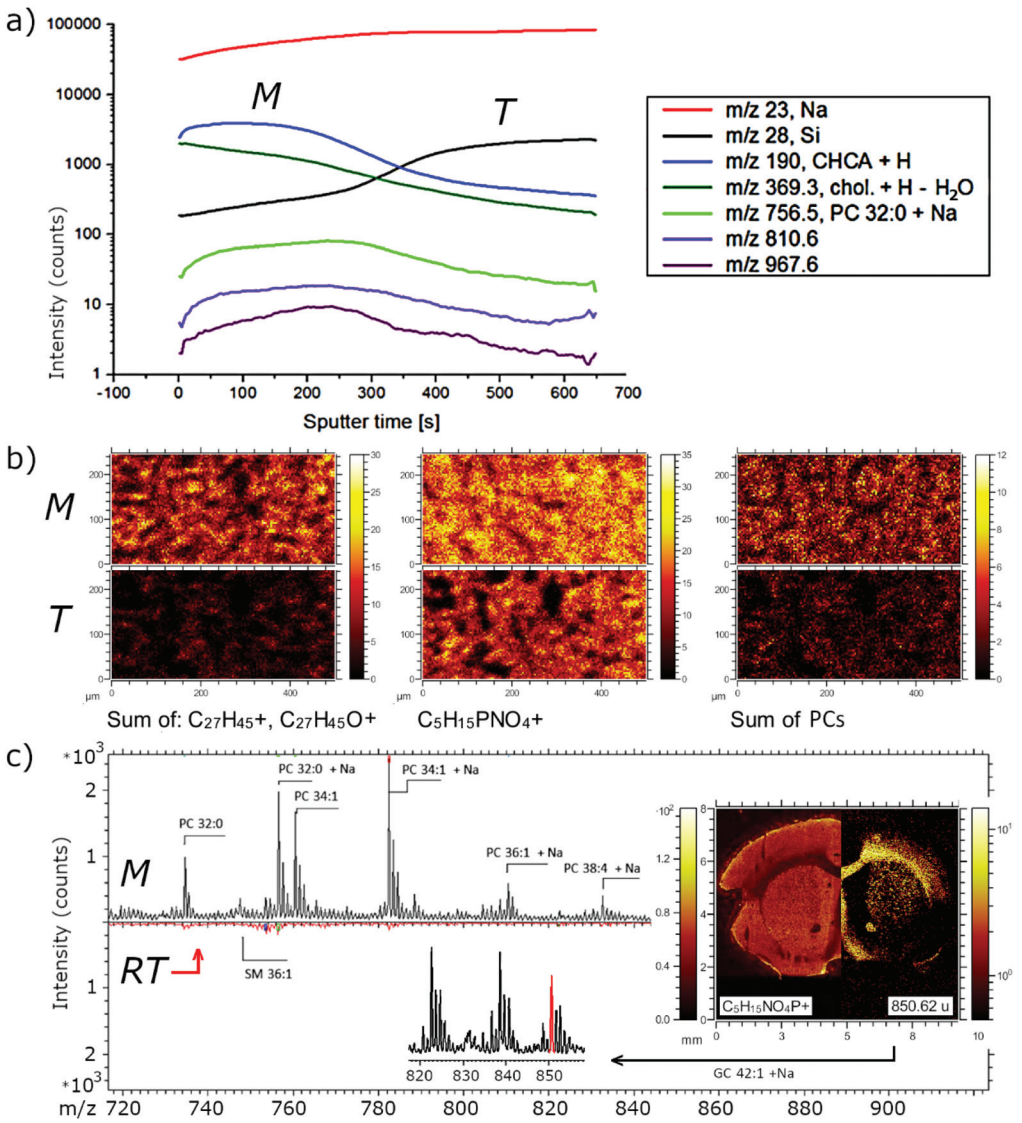

Fig. 10 (a) Positive ion depth profile of a brain tissue section with a transferred layer of CHCA (region of 500 × 500 μm^2 close to the target side). (b) Partial ion mappings reconstructed from the profiles (M, 0–300 s and T, 350–650 s) and (c) comparison of 720–850 *m*/*z* positive ion mass spectra of a brain section at the interface with CHCA (M, black spectrum) and a brain section reference (RT, red spectrum). Analysis beam fluences are respectively 1.41 × 10^{10} and 1.52 × 10^{10} ions per cm^2. Inset: Mosaic image of the complete brain section with transferred CHCA; left, phosphocholine headgroup; right, galactocerebroside 42 : 1.

right-hand side.[25,56,57] The left-hand side indicates the complementary localization of the phosphocholine headgroup from the same tissue section. Our preliminary studies of mouse brain tissue sections with sublimated matrix suggest that the potential for signal enhancement is even larger with 2,5-DHB than CHCA. However, because of its competitive sublimation in an ultra-high vacuum, it is trickier to obtain a sufficient and controlled transferred layer at room temperature than with CHCA. For more volatile matrices such as 2,5-DHB, sample cooling might be required.

In general, our results show that the enhancement of the molecular and/or characteristic ion signals strongly depends on the diffusion of the analyte in the matrix, which itself depends on the analyte molecule of interest in the tissue section, on the selected matrix, and on time and temperature. The profile of Fig. 10a indicates that, under the considered conditions, the diffusion of the large lipids provides a maximum intensity close to the interface of CHCA with the tissue, and less intensity at the top matrix surface. Therefore, in future experiments, in addition to the investigation of even better matrices for SIMS, the matrix layer deposition should also be accurately controlled to provide just the needed thickness for maximum enhancement. In this manner, the enhancement should be optimized for direct imaging of the surface, without the need for depth profiling. Note that this optimal thickness will probably vary as a function of the considered matrix, as our preliminary comparisons between CHCA and DHB suggest. Finally, sample imaging using large Ar_n^+ clusters instead of Bi_{3-5}^+ clusters will provide another degree of freedom, since the imaging analysis fluence can be tuned beyond the static limit without damage to the sample.

4. Conclusions

Data on the signal enhancement of various classes of biological molecules (lipids, sugars, peptides and metabolites) have been collected after *in situ* sputter-transfer of a MALDI matrix layer onto the samples of interest. The general trend is that the detection of species with naturally good detection efficiency in SIMS (angiotensin, D-serine, D-glutamic acid and cholesterol) does not benefit from the matrix overlayer, especially if these species are present as a concentrated layer. For considerably lower concentrations, the matrix overlayer may still improve the detection of some of these species (D-serine, D-glutamic acid), and for those that are barely detected by SIMS the transferred matrix layer provides a powerful boost of detection (up to two orders of magnitude and more), sometimes even enabling the detection in a depth-profiling mode (cardiolipin). The matrix effect is facilitated even for layers of *ca.* 50 nm matrix thickness, which are inaccessible to MALDI, as well as for concentrations below the MALDI capability, *e.g.* layers of a few to twenty nanometers. Considering SIMS imaging applications, this thin matrix layer arrangement should be quite beneficial as it should prevent the blurring of the mass-image induced by species diffusing through larger matrix crystals.

The field of application of the *in situ* matrix transfer technique can be expanded to organic tissues and especially frozen tissues, where even the matrix sublimation is not possible due to the proximity of the hot crucible and the temperature of the matrix vapor. Our preliminary experiments on cryo-preserved mouse brain slices are promising, even though the search for a better matrix for *in situ* ME-SIMS is still in progress. The geometry of the presented experiment, limited by the existing ToF-SIMS instrument constraints, might not be optimal for matrix transfer and matrix sputtering might be improved with a dedicated setup (sputtering time, thickness uniformity).

In this study, the SIMS analyses were performed without electron flooding in order to minimize the possible degradation of organic species and, interestingly, it demonstrated the ability to collect signals from surfaces that were charging in the absence of the matrix (maltoheptaose). Combining these possibilities, depth profile experiments could provide two types of datasets complementing each other – one obtained by the MALDI matrix-assisted ionization in the absence of electron beam and one generated by the sputtering of the pristine sample with electron charge compensation.

Finally, the highest sensitivity enhancements were measured by the integration of the signals upon molecular depth-profiling of the matrix layer, at variance with the static SIMS analyses generally reported in the ME-SIMS literature. This observation suggests that the best advantage of *in situ* ME-SIMS might be obtained from instruments that capitalize on the use of gas cluster ion beams (IONTOF OrbiSIMS, Ionoptika J105).

Author contributions

K. M. designed the sublimation chamber, the new sample holder for molecular transfer and he conducted all the experiments of *in situ* ME-SIMS on model biomolecules. B. T. and T. D. performed the analysis of brain tissue sections. V. D. contributed to the design and first experiments of molecular transfer at UCLouvain. K. V. and V. P. prepared and provided us with mouse brain tissue sections embedded in resin. M. L. provided the first sample holder and participated in the discussion of the results. J. Q. acquired the MALDI MS data and analyzed/discussed them with G. B. and F. L. C. D. and A. D. instigated and supervised the project involving molecular transfer. K. M. and A. D. wrote the article.

Conflicts of interest

There are no conflicts of interest to declare.

Acknowledgements

This research, K. M., B. T. and T. D. were supported by the Fédération Wallonie Bruxelles, through the project "iBEAM" funded by its research program "Actions de Recherche

Concertées" (contract no. 18-23-090). M. L. was funded by the OrbiSIMS project in the Life-Sciences and Health programme of the National Measurement System of the UK Department of Business, Energy and Industrial Strategy. A. D. is the Research Director of the Fonds National de la Recherche Scientifique (FNRS) of Belgium. The authors are grateful to Ian Gilmore at the NPL for lending their matrix transfer sample holder and for useful discussions.

References

1 M. Karas and F. Hillenkamp, *Anal. Chem.*, 1988, **60**, 2299–2301.
2 Z. Takats, J. M. Wiseman and R. G. Cooks, *J. Mass Spectrom.*, 2005, **40**, 1261–1275.
3 A. Delcorte, Ch. Leblanc, C. Poleunis and K. Hamraoui, *J. Phys. Chem. C*, 2013, **117**, 2740–2752.
4 S. Ninomiya, Y. Nakata, K. Ichiki, T. Seki, T. Aoki and J. Matsuo, *Nucl. Instrum. Methods Phys. Res., Sect. B*, 2007, **256**, 493–496.
5 T. Mouhib, C. Poleunis, N. Wehbe, J. J. Michels, Y. Galagan, L. Houssiau, P. Bertrand and A. Delcorte, *Analyst*, 2013, **138**, 6801–6810.
6 N. Winograd, *Annu. Rev. Anal. Chem.*, 2018, **11**, 29–48.
7 M. K. Passarelli, A. Pirkl, R. Möllers, D. Grinfeld, F. Kollmer, R. Havelund, C. F. Newman, P. S. Marshall, H. Arlinghaus, M. R. Alexander, A. West, S. Horning, E. Niehuis, A. Makarov, C. T. Dollery and I. S. Gilmore, *Nat. Methods*, 2017, **14**, 1175–1183.
8 V. R. Deline, W. Katz, C. A. Evans and P. Williams, *Appl. Phys. Lett.*, 1978, **33**, 832–835.
9 R. G. Cooks and K. L. Busch, *Int. J. Mass Spectrom. Ion Phys.*, 1983, **53**, 111–124.
10 E. A. Jones, N. P. Lockyer and J. C. Vickerman, *Int. J. Mass Spectrom.*, 2007, **260**, 146–157.
11 K. Mizomichi, T. Yamagishi, T. Kawashima, M. Dürr and S. Aoyagi, *Biointerphases*, 2020, **15**, 021008.
12 I. S. Gilmore, S. Heiles and C. L. Pieterse, *Annu. Rev. Anal. Chem.*, 2019, **12**, 1–24.
13 M. Z. Huang, H. J. Hsu, C.-I. Wu, S.-Y. Lin, Y.-L. Ma, T.-L. Cheng and J. Shiea, *Rapid Commun. Mass Spectrom.*, 2007, **21**, 1767–1775.
14 P. Nemes and A. Vertes, *Anal. Chem.*, 2007, **79**, 8098–8106.
15 A. Pelster, M. Körsgen, M. Heeger and H. F. Arlinghaus, *J. Phys. Chem. C*, 2017, **121**, 15266–15271.
16 K. A. Moshkunov, S. S. Alimpiev, A. A. Grechnikov, S. M. Nikifirov, A. V. Pento and Y. O. Simanovsky, *J. Phys.: Conf. Ser.*, 2014, **558**, 012012.
17 Y. Xiao, J. Deng, Y. Yao, L. Fang, Y. Yang and T. Luan, *Anal. Chim. Acta*, 2020, **1117**, 74–88.
18 N. Mine, B. Douhard, J. Brison and L. Houssiau, *Rapid Commun. Mass Spectrom.*, 2007, **21**, 2680–2684.
19 A. Delcorte and P. Bertrand, *Anal. Chem.*, 2005, **77**, 2107–2115.
20 T. M. Brewer, Ch. Szakal and G. Gillen, *Rapid Commun. Mass Spectrom.*, 2010, **24**, 593–598.
21 X. A. Conlan, N. P. Lockyer and J. Vickerman, *Rapid Commun. Mass Spectrom.*, 2006, **20**, 1327–1334.
22 A. Delcorte, N. Médard and P. Bertrand, *Anal. Chem.*, 2002, **74**, 4955–4968.
23 A. Delcorte, J. Bour, F. Aubriet, J.-F. Muller and P. Bertrand, *Anal. Chem.*, 2003, **75**, 6875–6885.
24 T. Mouhib, A. Delcorte, C. Poleunis and P. Bertrand, *J. Am. Soc. Mass Spectrom.*, 2010, **21**, 2005–2010.
25 T. B. Angerer, M. Dowlatshahi Pour, P. Malmberg and J. S. Fletcher, *Anal. Chem.*, 2015, **87**, 4305–4313.
26 K. Wittmaack, W. Szymczak, G. Hoheisel and W. Tuszynski, *J. Am. Soc. Mass Spectrom.*, 2000, **11**, 553–563.
27 A. Delcorte, *Appl. Surf. Sci.*, 2006, **252**, 6582–6587.
28 K. J. Wu and R. W. Odom, *Anal. Chem.*, 1996, **68**, 873–882.
29 S. Van Nuffel, N. Elie, E. Yang, J. Nouet, D. Touboul, P. Chaurand and A. Brunelle, *Anal. Chem.*, 2018, **90**, 1907–1914.
30 J. E. Locklear, C. Guillermier, S. V. Verkhoturov and E. A. Schweikert, *Appl. Surf. Sci.*, 2006, **252**, 6624–6627.
31 M. Karas and F. Hillenkamp, *Anal. Chem.*, 1988, **60**, 2299–2301.
32 L. A. McDonnell and R. M. A. Heeren, *Mass Spectrom. Rev.*, 2007, **26**, 606–643.
33 S. L. Luxembourg, L. A. McDonnell, M. C. Duursma, X. Guo and R. M. A. Heeren, *Anal. Chem.*, 2003, **75**, 2333–2341.
34 A. Thomas, J. Laveaux Charbonneau, E. Fournaise and P. Chaurand, *Anal. Chem.*, 2012, **84**, 2048–2054.
35 S. Sheraz née Rabbani, A. Barber, J. S. Fletcher, N. P. Lockyer and J. C. Vickerman, *Anal. Chem.*, 2013, **85**, 5654–5658.
36 S. Sheraz née Rabbani, I. B. Razo, T. Kohn, N. P. Lockyer and J. C. Vickerman, *Anal. Chem.*, 2015, **87**, 2367–2374.
37 A. Wucher, H. Tian and N. Winograd, *Rapid Commun. Mass Spectrom.*, 2014, **28**, 396–400.
38 H. Tian, A. Wucher and N. Winograd, *Biointerphases*, 2016, **11**, 02A320.
39 M. Lorenz, A. G. Shard, J. D. P. Counsell, S. Hutton and I. S. Gilmore, *J. Phys. Chem. C*, 2016, **120**, 25317–25327.
40 M. Lorenz, J. Zhang, A. G. Shard, J.-L. Vorng, P. D. Rakowska and I. S. Gilmore, *Anal. Chem.*, 2021, **93**, 3436–3444.
41 A. Delcorte, V. Delmez, Ch. Dupont-Gillain, C. Lauzin, H. Jefford, M. Chundak, C. Poleunis and K. Moshkunov, *Phys. Chem. Chem. Phys.*, 2020, **22**, 17427–17447.
42 V. Delmez, H. Degand, C. Poleunis, K. Moshkunov, M. Chundak, Ch. Dupont-Gillain and A. Delcorte, *J. Phys. Chem. Lett.*, 2021, **12**, 952–957.
43 https://med.nyu.edu/research/scientific-cores-shared-resources/sites/default/files/frozen-tissue-preparation-with-sucrose.pdf.
44 S. Yoon and T. G. Lee, *Nano Convergence*, 2018, **5**(24), 1–13.
45 L. A. McDonnell, T. H. Mize, S. L. Luxembourg, S. Koster, G. B. Eijkel, E. Verpoorte, N. F. de Rooij and R. M. A. Heeren, *Anal. Chem.*, 2003, **75**, 4373–4381.
46 https://sunchrom.de/maldi-imaging-3/.

47 M. Körsgen, A. Pelster, S. Vens-Cappell, O. Roling and H. F. Arlinghaus, *Surf. Interface Anal.*, 2016, **48**, 34–39.
48 M. P. Seah, *J. Phys. Chem. C*, 2013, **117**, 12622–12632.
49 P. J. Cumpson, J. F. Portoles and N. Sano, *J. Vac. Sci. Technol., A*, 2013, **31**, 020605–020601.
50 T. Seki, T. Murase and J. Matsuo, *Nucl. Instrum. Methods Phys. Res., Sect. B*, 2006, **242**, 179–181.
51 P. Malmberg, H. Nygren, P. Sjövall and J. Lausmaa, *Spectroscopy*, 2004, **18**, 503–511.
52 R. Knochenmuss, A. Stortelder, K. Breuker and R. Zenobi, *J. Mass Spectrom.*, 2000, **35**, 1237–1245.
53 A. Brunelle and O. Laprévote, *Curr. Pharm. Des.*, 2007, **13**, 3335–3343.
54 M. Dowlatshahi Pour, P. Malmberg and A. Ewing, *Anal. Bioanal. Chem.*, 2016, **408**, 3071–3081.
55 P. Sjövall, B. Johansson and J. Lausmaa, *Appl. Surf. Sci.*, 2006, **252**, 6966–6974.
56 M. K. Passarelli and N. Winograd, *Biochim. Biophys. Acta*, 2011, **1811**, 976–990.
57 A. S. Mohammadi, N. T. N. Phan, J. S. Fletcher and A. G. Ewing, *Anal. Bioanal. Chem.*, 2016, **408**, 6857–6868.